Chemical and mechanical performances of CVD-silicon oxycarbonitride films for corrosion protection applications: Towards inert coatings in aggressive aqueous media

Farah Inoubli, Babacar Diallo, Konstantina Christina Topka, Raphael Laloo, Brigitte Caussat, Thierry Sauvage, Viviane Turq, Nadia Pellerin

Chemical and mechanical performances of CVD-silicon oxycarbonitride films for corrosion protection applications: Towards inert coatings in aggressive aqueous media

Farah Inoubli[1,2,3], *Babacar Diallo* [1,2,3], *Raphael Lalo* [5,7,8,7], *Konstantina Christina Topka*[4], *Emmanuel Veron*[1,3], *Constantin Vahlas*[5,7,8,7], *Brigitte Caussat* [6,7,8,7], *Thierry Sauvage* [1,2,3], *Viviane Turq*[5,7,8,7], *Nadia Pellerin*[1,2,3,*].

[1]Conditions Extrêmes et Matériaux : Haute Température et Irradiation (CEMHTI), Orléans, F-45100 France

[2] Université d'Orléans, Orléans, F-45100 France

[3] CNRS, délégation Centre Limousin Poitou Charente, Orléans, F-45100 France

[4] Air Liquide Japan, Innovation Campus Tokyo, 2-2 Hikari-no-oka, Yokosuka-shi, Kanagawa, 239-0847 Japan

[5]Centre Interuniversitaire de Recherche et d'Ingénierie des Matériaux (CIRIMAT), Toulouse, F-31062 France

[6]Laboratoire de Génie Chimique (LGC), Toulouse, F-31062 France

[7] INP, Toulouse, F-31400 France

[8] Université Toulouse III, Toulouse, F-31062 France

[9] CNRS, délégation Occitanie Ouest du CNRS, Toulouse, F-31062 France

* Co-corresponding author. Email: nadia.pellerin@univ-orleans.fr

KEYWORDS: silicon oxide coatings; corrosion barrier; Chemical vapor deposition; IBA; FTIR.

Abstract

This study investigates the alteration behaviour of three CVD amorphous silica thin films deposited at three different deposition temperatures, exhibiting thus different network qualities. The hydrolysis of the networks was elucidated through ERDA hydrogen depth profiles acquired throughout the alteration process. It is worth noting that this hydrolysis is insignificant since a maximum of hydrogen atomic concentration of 10% was recorded during all the study. It was also evinced that the concentration and distribution of hydrogen throughout the depth are influenced by two competing phenomena: hydrolysis and ionic exchange of protons with K^+ ions coming from the solution. This competition is particularly noticeable in the film deposited at the lowest investigated temperature, where the presence of sufficiently large voids facilitates this exchange. Thickness loss rates were successfully calculated showing remarkably low initial rates ranging from 2.5 to 4.8 nm/day, directly correlated with the initial network quality. A residual rate as low as 0.5 nm/day was recorded, indicating limited hydration and hydrolysis mechanisms leading to the release of H_4SiO_4, given the higher dissociation energy required for such polymerized networks. These findings represent the first available dataset on dissolution rates of CVD-deposited silica films. It was demonstrated that network dissolution occurs evenly across the entire surface since the measured RMS values post-alteration remain quite low with a maximum of 2 nm. Finally, our study was supported by nanoindentation tests to assess hardness and elasticity, revealing a decrease of 38% and 13%, respectively, which was attributed to the high sensitivity of these two properties to physicochemical changes, particularly on the surface, during alteration. This comprehensive investigation has facilitated the accurate correlation of CVD deposition conditions and, consequently, the network quality of silica films to the chemical and mechanical response to aqueous alteration.

Introduction

Amorphous silica thin films are nowadays of major importance due to their involvement in many technological fields such as optical coating applications, semiconductor devices, as well as chemical protective coatings on glass [1-3]. These materials are of prime interest thanks to their excellent mechanical properties, their high corrosion resistance but also thanks to their refractory properties [4-6].

Preparation of amorphous silica thin films by chemical vapour deposition (CVD) process is very attractive, as it allows their synthesis at relatively low temperature and under atmospheric pressure, which makes it an inexpensive method [7]. It also permits the exploration of many chemical pathways leading to film formation. Tetraethyl orthosilicate ($Si(OC_2H_5)_4$, TEOS) is a very popular precursor widely used to produce this material [8-9]. Yet, the quality of deposited films is still arguable since defects, including silanols Si-OH or Si-H bonds, can occur notably for deposition temperatures below 450°C [10-12]. Adding oxidants to the gas phase, such as oxygen and ozone mixtures, can deeply enhance the process by empowering the oxidation of TEOS and reducing the deposition temperature [5; 13; 14]. Recently, K. Topka et al. have combined experimental data taken from an atmospheric pressure Chemical Vapor Deposition hot-wall reactor with horizontal configuration and Computational Fluid Dynamics (CFD) simulation to understand the kinetics and chemical mechanisms behind SiO_2 deposition from TEOS and O_2/O_3 oxidizing atmosphere. They asserted that ozone injection in the reactor is a key to improve the yield and the precursor conversion [13]. B. Diallo et al have shown that ozone allows increasing the structural and chemical quality of SiO_2 films [15]. In the same study, they have confirmed the improvement of the chemical and structural quality of films at higher deposition temperatures (Td), explaining this enhancement as a consequence of a dehydration-condensation mechanism leading to lower amount of hydration species and stronger network connectivity. Young modulus and hardness were also examined on these thin coatings. These parameters remain stable in the investigated range of temperature (450 to 550°C) at 64.2 ± 1.7 and 7.4 ± 0.3 GPa respectively [15]. Such characterizations are very important to evaluate the films quality and to predict their durability. However, a comprehensive evaluation of the performance can only occur when the response of the material to external disturbances is investigated. Indeed, many studies were dedicated to silica and silicate glasses chemical durability [16,17]. The diffusion, hydration and hydrolysis phenomena that yield to the glass leaching are well described, although the debate is still open on the models of alteration and the kinetics behind, given their complexity and the dependence on numerous experimental parameters. Most of these studies were carried out on bulk materials (powder or monolith) where the best results were found using nuclear glasses with initial dissolution rates range between 0.3−8.2 $g \cdot m^{-2}$/day [18]. However, few studies are done on films and layers. Ponton et al. and Diallo et al., for instance [5, 15], adopted the P-etch test developed by Pliskin to evaluate CVD-silica films corrosion resistance in hydrofluoric acid [19]. Their results show a decrease by half of the etching rate for Td varying between 400 and 550°C, reaching 10 $A.s^{-1}$ in a very acidic medium (pH = 1.5). However, their experiment durations were very short and cannot be truly representative of the chemical durability of the tested materials or report on the corrosion resistance of these coatings under real application conditions, in various aqueous media [5, 15].M. Klause et al. have studied the dissolution behaviour of SiO_2-coatings deposited by plasma enhanced chemical vapor deposition using a pulsed microwave plasma (PICVD) from hexamethyldisiloxane precursor (HMDSO). They rely on thickness loss to calculate silica dissolution rates under different pH (5.5 and 7) and temperatures (60

and 90°C), assuming that the rate depends linearly on time. The rates vary between 0.1 and >50 nm/h, with a notable increase with pH and temperature [20].

The goal of this paper is to evaluate the short and medium-term chemical and mechanical performances of three films produced by CVD using the TEOS/O_2/O_3 chemical route at three different deposition temperatures (450, 500 and 550°C) by providing quantitative data and to discuss the performances as a function of the initial structural and chemical network quality. The investigation delves into the properties of the coatings when subjected to cycles of exposure to a weak acidic aqueous solution at high temperature. Using Ion Beam Analysis (IBA) techniques, we meticulously examine the extent of alteration via chemical changes. These techniques are employed before and throughout the alteration process to precisely track variations in elemental composition, including hydrogen, as well as film thickness. Additional insights into composition are provided by Time-of-Flight Secondary Ion Mass Spectrometry (TOF-SIMS). Fourier Transform Infrared (FTIR) spectroscopy is employed to detect structural changes, offering direct insights into molecular and submolecular structures, alongside valuable data on hydrated species [21-25]. Complementing this, 1H solid-state Nuclear Magnetic Resonance (NMR) aids in distinguishing the different forms of hydration species. The surfaces of the films are scrutinized through Atomic Force Microscopy (AFM) and Scanning Electron Microscopy (SEM). Lastly, nanoindentation tests are conducted to identify changes in mechanical properties and establish correlations with the network state, thereby bolstering the comprehensive nature of our study.

Experimental section

1-Film synthesis

Silica films were produced in a horizontal tubular hot-wall CVD reactor with a reaction chamber of 700 mm long quartz tube, described in previous works [13, 15]. The experiments have been carried out at three different deposition temperatures namely 450°C (sample A), 500°C (sample B) and 550°C (sample C), corresponding to the temperature measured in the second half of the reactor where an isothermal regime is established in a region of around 140 mm. TEOS and O_2/ O_3 flow rates were respectively 2 standard cubic centimetres per minute (sccm) and 1960 sccm, for O_3 concentration of 60 mg/L.

280 µm thick monocrystalline silicon wafers cut in rectangles of 32 X 24 mm^2, were used as substrates. They were put vertically in a substrate holder placed in the isothermal region spanning approximately from 360 to 500 mm from the reactor inlet. An average deposition time of 300 minutes results in films with a thickness ranging from 377 to 750 nm depending on the used temperature.

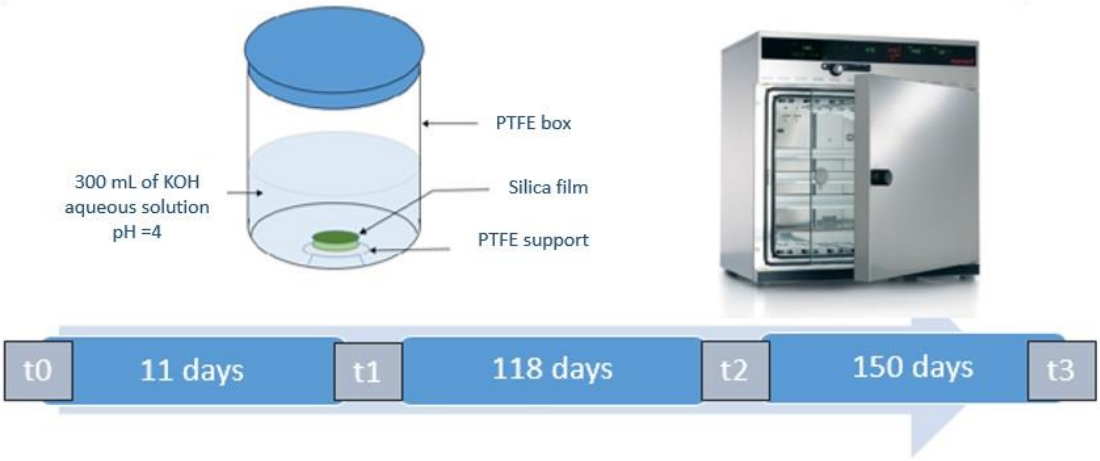

Figure 1: Alteration steps of silica films.

Table1: Deposition temperature and corresponding film thickness.

Film	A	B	C
Deposition temperature (°C)	**450**	**500**	**550**
Thickness (nm) converted from RBS results	**377 ± 1.4**	**543 ± 1.4**	**750 ± 1.4**

2- Alteration experiments

Aqueous solution of potassium hydroxide with mass concentration of 0.055 $g.L^{-1}$ was used for the alteration experiments. The pH was adjusted to 4 by adding few drops of sulphuric acid. The solid-liquid system was put in a closed Teflon® box placed in a standard laboratory oven set at 90°C to accelerate the process [26]. The film surface area to solution volume ratio was equal to 2 m^{-1}. In total, three successive alteration cycles were done. At first, an explorative test of 11 days to inspect the response of the films to these chemical conditions, followed by two other longer sequences that lasted respectively 118 and 150 days. The last alteration experiment took place in a renewed solution to accelerate the etching. After each alteration sequence, the sample is rinsed with ultra-pure water and then left outdoors until completely dry. In the following, the notation t_0 will be used to refer to analyses on pristine films, while t_1, t_2, and t_3 will represent analyses after 11, 129, and 279 days of exposure to the aqueous solution.

3- Characterization techniques

Ion Beam Analysis (IBA) was performed to determine the chemical composition of the films. Silicon, oxygen and hydrogen contents were obtained by combining Rutherford Backscattering Spectroscopy (RBS) and Elastic Recoil Detection Analysis (ERDA). A 2.8 MeV $^4He^+$ beam from a Pelletron accelerator was used for both RBS and ERDA with corresponding detectors positioned at 155° and 30° angles to

the ion beam axis. All the spectra were simulated using SIMNRA software [27]. For energy calibration of the RBS detector, three distinct samples were utilized: a silicon substrate with a top layer of 213 nm SiO_2 film, a silicon substrate with a 213 nm SiO_2 layer onto which a gold (Au) layer was deposited and a cobalt (Co) layer on top of silicon substrate. To ensure the quantitative accuracy of ERDA analysis, a-SiH hydrogen standard at 2.19 x 10^{17} H/cm^2 was consistently employed to validate the cross section of the $^1H(^4He,^1H)^4He$ nuclear reaction.

Film thickness is calculated by SIMNRA and is expressed in 10^{15} atoms.cm^{-2}. To convert this measurement to nm, we use the mathematical expression below assuming that all films have a density ρ of 2.2 g/cm^3.

$$\boldsymbol{Thickness\ (nm) = \frac{10^7\ .\ thickness\ (10^{15}\ \ atoms.cm^{-2}\ ).\ Molar\ mass}{\varrho.NA}} \quad (1)$$

The depth concentration profiles for hydrogen relies on the concept of depth resolution in our analysis conditions. This refers to the smallest distance needed to detect a contrast in H concentration between two consecutive sub-layers. For SIMNRA simulation of the experimental ERDA spectrum, the sample is virtually cut in SiO_2 sublayers for which we can adjust the hydrogen concentration. It hinges on factors such as the minimum detectable energy difference and the material's stopping power. Following the methodology outlined by Martin et al.[28], we determined the depth resolution of hydrogen within silica films to a value of 430 10^{15} at/cm², corresponding to xx?? nm.

Complementary analyses by TOF-SIMS were performed using an IONTOF TOF 5 instrument. An Ar^+ ion beam of 20 keV and 12 nA was used for surface abrasion (500 x 500 µm^2). The analysis was then provided by a Bi_3^+ ion sputtering beam (25 keV, ~0.2 pA, 100 x 100 µm^2) to investigate by ToF the secondary ions extracted from the samples. The surface was neutralized during analysis by a low-energy electron flux (<20 eV). The depth of the final crater was measured using a 3D profilometer, allowing elemental profile depth calibration. The following species profiles were selected for analysis: Si^+, SiO^+, $SiHO^+$, H^+ and K^+.These profiles were then normalized to that of Si^+ to avoid matrix effects, taking into account the low mobility and the abundance of silicon. The following formula was used for this purpose:

$$Jn_i^a = {J_i^a}/{J_i^{Si^+}} \quad (2)$$

Where Jn_i^a is the normalized intensity of an element a, and J_i^a and $J_i^{Si^+}$ are the as-measured intensities at a point i of the profile for the elements a and Si^+.

Structural information was provided by a Thermo Scientific «Nicolet is 10» FTIR spectrometer. All spectra were recorded in a transmission mode at normal incidence and at 60° off-normal, to facilitate separation of the TO band from its corresponding LO [29-30]. The spectral range between 400-4400 cm^{-1} was probed with a resolution of 4 cm^{-1}. Thirty-two spectra accumulations were taken for each sample. After acquisition, baseline corrections were performed using OMNIC software followed by the removal of silicon substrate signal. NMR spectroscopy characterization was performed only on the altered sample A (t_3). Signals, obtained from ^{1}H Hahn echomas pulse sequences with different echo

delays going from 218.3 to 2018.9 µs, were collected with a Bruker Avance 750 MHz spectrometer with a magnetic field of 17.62 T. A 4 mm probe was used for this purpose, allowing us to work at 10 kHz spinning rate. The best signal to noise ratio was obtained with the shorter echo delay that will be presented in this work. ^{1}H chemical shifts were referenced with tetramethylsilane at 0 ppm.^{1}H NMR signal deconvolution was performed using DMfit program [31], considering a Gaussian model line. Microstructure of the films was analysed by means of a «JEOL JSM-IT800» Scanning Electron Microscope (SEM) equipped with Scintillator Backscattered Electron Detector (SBED). Since SEM imaging is performed under vacuum, a small piece was cut from film A at t_3 and was dedicated to this analysis to avoid any change induced by vacuum. The surface roughness was measured using a Bruker Dimension ICON, BRUKER, Nanoscope V Atomic Force Microscope (AFM) working with tapping mode. A surface of 1x1 µm^2 was scanned for all the measurements. Finally, mechanical properties i.e. Young modulus and hardness were evaluated using an ultra nano indenter apparatus from CSM Instruments with a Berkovich diamond indenter and with ultra-low thermal drift thanks to the utilization of passive surface referencing. For nanoindentation, the load was gradually increased until a maximum value of 0.5 mN, at which it was maintained for 30 s, and then decreased down to zero. The loading and unloading rate was 1 mN/min. The system has typical load and displacement resolutions of 0.25 mN and 0.1 nm respectively. Elastic modulus and hardness were calculated from the load vs. depth curves with the method proposed by Oliver and Pharr [4]. A fixed indentation depth of 70 nm was used for all the films performed using a Berkovich diamond indenter. At this indentation depth, we assume that the contribution of silicon substrate in the measurements is wholly eliminated [32].

Results

1- <u>Chemical composition and Structure</u>

Figure 2A shows the RBS spectra for sample A (deposited at 450°C), recorded at different times (t_0, t_1, t_2 and t_3) throughout the alteration experiment. A significant evolution of the spectra is observed marked by the reduction in width of both plateaus corresponding to the elements of the film: Si (grey area) and O (green area) throughout alteration. These coupled phenomena denote progressive silica thickness reduction. This evolution is observed for all the films with a sample-dependent intensity. The loss was quantified by means of SIMNRA software simulations. Thickness loss after t_3 alteration time was found to be more pronounced for low temperature-deposited films,157 ± 1.4 nm is obtained for film A against 151 ± 1.4 nm for sample B and only 141 ± 1.4 nm for sample C (table 2). It is worthy to note that a variation in film thickness of ± 2 nm around the optimized value (best simulation of the experimental RBS spectrum) affects the quality of the simulation and can be perceived as an under or over estimation of film's thickness.. Thus, errors in thickness measurements by RBS are estimated to within 2 nm. Figure2b exposes thickness loss rate curves of all analysed films. For the three samples, two main stages are identified. An initial and expected fast stage taking place during the first days of exposure characterized by a high rate going from 4.8 nm/day for A to 2.5 nm/day for C. After that, between t_1 and t_3, an important drop is recorded for all the samples and the rate stabilizes during the rest of the exposure at 0.5 nm/day for A and B, and 0.4 nm/day for C.

Data obtained from ERDA analysis for each film between t_0 and t_3 are illustrated in figure 3 that shows the depth profile evolution of hydrogen contents (at.%). The graph confirms the thickness loss already

observed by RBS for all the samples and its Td dependence. Concerning hydrogen content, figure 3 reveals that for pristine films (blue curves), the higher the deposition temperature, the lower the hydrogen content with average values of 7.2± 0.2%, 5.8± 0.2% and 4.3± 0.1%, respectively for A, B and C (table 2). The profile shapes for B and C are quite similar, exhibiting a maximum concentration of H near the surface, which decreases gradually with depth. However, in the case of A, the maximum concentration is situated in the middle depth of the coating, presenting a bell curve profile across the layer. During the first alteration cycle, the three films adopt the same alteration behavior by accumulating more hydrogen atoms between t_0 and t_1 (orange curves). The apex of the curve shifts marginally towards greater depth for both A and B, whereas in the case of C, there is no noticeable shift, indicating a consistent concentration of H throughout the film. In C, the H profile is distinguished by a significant decrease across the film, underscoring the limited diffusion of protons. At t_2 and t_3, the thickness loss is combined with hydrogen levels decrease in A, whereas for B there is no significant profile evolution to note except the change of H content at the extreme surface. For C however, hydrogen concentration remains stable between t_1 and t_2 and then resumed the rise between t_2 and t_3. Finally, despite of the long period of contact with the aqueous solution, the films still exhibit quite low concentration in hydrogen, with average values along the profile of 7.13± 0.24%, 8.17± 0.26% and 6.74± 0.21% respectively for A,B and C at t_3. Hydrogen profiles show also that small amounts (lower than 5 at.%) diffuse into the substrate.

TOF-SIMS depth profiling of the films obtained at t_3, exhibited in figure 4, evidences the good quality of the silica films with homogeneous Si^+ and SiO^+ signals into the coating after alteration regardless of Td. The slope of the signals observed in figure 4b and 4c is considered to be an artefact linked to acquisition, given the slope of the Si signal. The SiO^+ and $SiOH^+$ normalized signals are regular along the thickness for the three coatings. Table 3 shows the decrease with Td of the intensity ratio $SiOH^+/SiO^+$ as expected, from 0.61 for sample A to 0.49 for sample C. Penetration of potassium in the silica network coming from the solution has been spotted. While B and C samples exhibit high K^+ surface concentration profiles followed by a strong drop of the concentration up to an average level around 0.004 for sample B and 0.0005 for sample C, sample A shows a K^+ slight accumulation with a maximum appearing towards 20 nm at around 0.01 of intensity followed by a stabilization along the depth at around 0.009. As for hydrogen, TOF-SIMS shows very close amounts for A, B and C confirming thus the reliability of ERDA upshots. A notable correlation between the profiles of K^+ and H^+ is evident across all samples, where a decrease in H^+ coincides with an increase in K^+ concentration at the surface within the first few nanometers (observed in sample A) and in the deepest sections of the layer close to the film-substrate interface (observed in all samples),which supports the hypothesis of ionic exchange between the two cations. Sample A records the highest mean K^+ to H^+ intensity ratio (2.7) followed by B (0.9) while C has the lowest one (0.3).

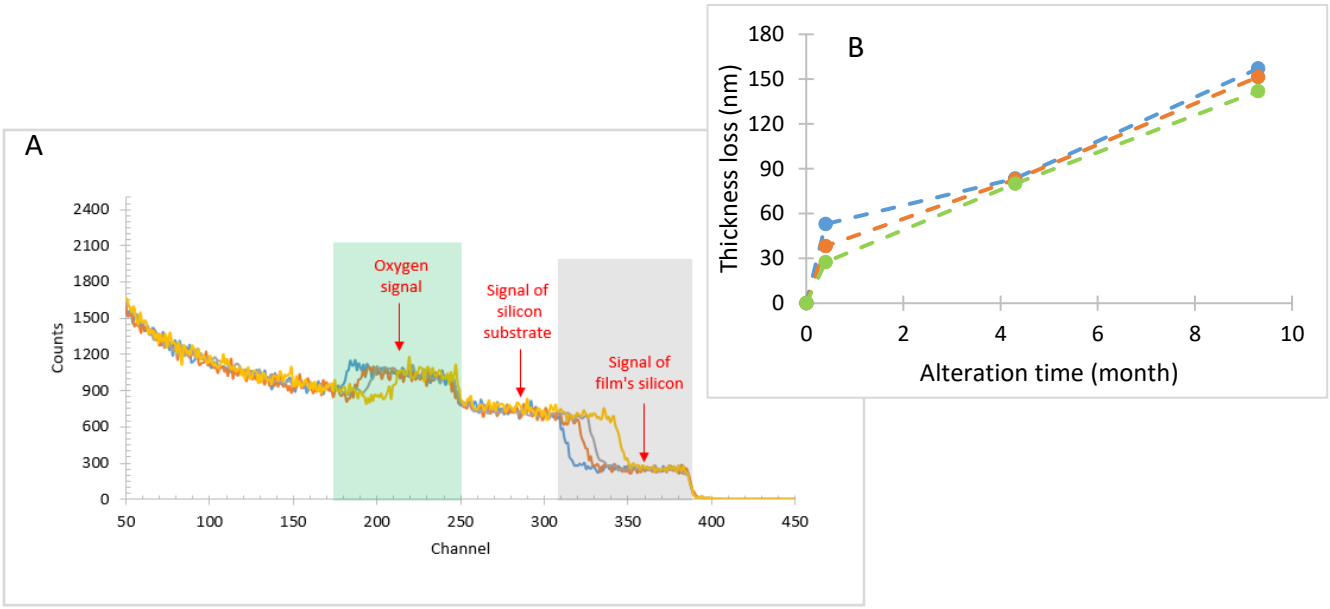

Figure 2: (A) RBS spectra of the film A recorded before alteration (t_0 blue curve), after the first cycle of alteration (t_1 orange curve), after the second cycle of alteration (t_2 grey curve) and at the end of the experiment (t_3 yellow curve).

(B) Evolution of thickness loss as a function of the duration of alteration for sample A (blue curve), B (orange curve) and C (green curve). The lines are just indicative guide for observation.

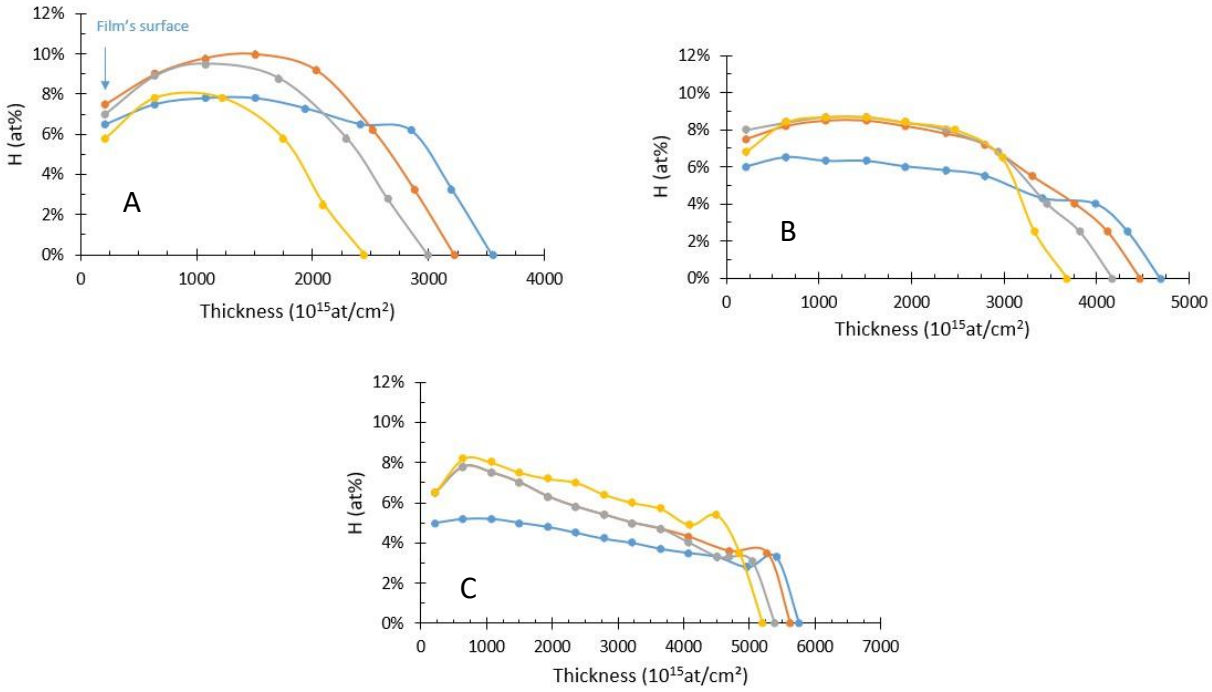

Figure 3: At.% H depth profiling before alteration (t_0, blue curves), after the first cycle of alteration (t_1, orange curves), after the second cycle of alteration (t_2, grey curves) and at the end of the experiment (t_3, yellow curves), A: coatingA, B: coating B, C: coating C.

Table2: Film thicknesses and composition evolution throughout alteration obtained from RBS and ERDA analysis.

Film A (450°C)					
Analysis time	**Film Thickness (10^{15}atm/cm²)**	**Thickness (nm)**	**%Si**	**%O**	**%H**
t0	**2675**	**377**	**31.09 ± 0.96**	**61.68 ± 1.92**	**7.23 ± 0.23**
t1	**2350**	**324**	**30.10 ± 0.94**	**60.80 ± 1.92**	**9.10 ± 0.29**
t2	**2120**	**293.62**	**30.00 ± 0.93**	**61.45 ± 1.94**	**8.55± 0.27**
t3	**1570**	**219.97**	**30.00 ± 0.97**	**62.87± 2.07**	**7.13± 0.24**
Film B (500°C)					
Analysis time	**Thickness(10^{15}atm/cm²)**	**Thickness(nm)**	**%Si**	**%O**	**%H**
t0	**3810**	**543**	**31.25 ± 0.95**	**62.91 ± 1.93**	**5.84 ± 0.18**
t1	**3590**	**504.85**	**31.25 ± 0.96**	**61.07 ± 1.89**	**7.68 ± 0.24**
t2	**3290**	**460.20**	**31.00 ± 0.96**	**60.86 ± 1.89**	**8.14 ± 0.25**
t3	**2800**	**391.56**	**31.00 ± 0.97**	**60.83 ± 1.94**	**8.17± 0.26**
Film C (550°C)					
Analysis time	**Thickness(10^{15}atm/cm²)**	**Thickness(nm)**	**%Si**	**%O**	**%H**
t0	**5230**	**750**	**30.08 ± 0.92**	**65.65 ± 2.01**	**4.25 ± 0.13**
t1	**5100**	**722.59**	**30.09 ± 0.92**	**64.10 ± 1.96**	**5.81 ± 0.18**
t2	**4730**	**670.10**	**30.00± 0.91**	**64.25 ± 1.97**	**5.75 ± 0.18**
t3	**4330**	**608.19**	**29.90± 0.92**	**63.63 ± 1.96**	**6.74 ± 0.21**

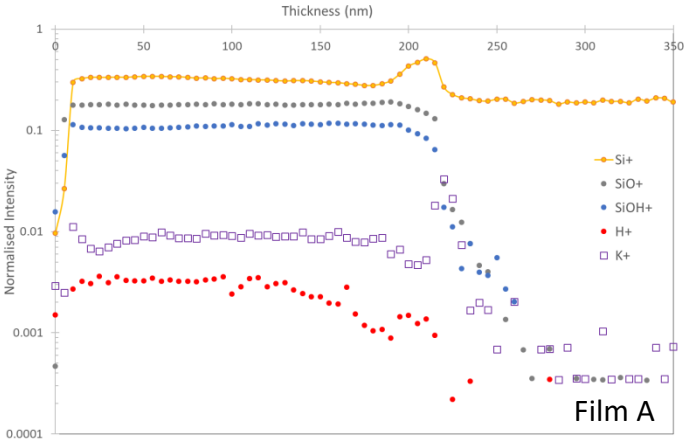

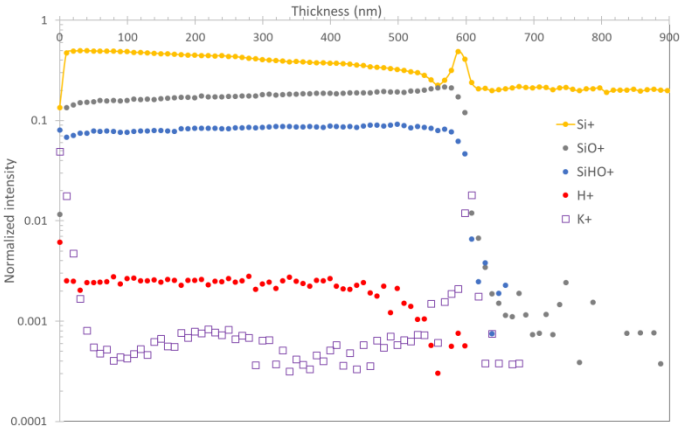

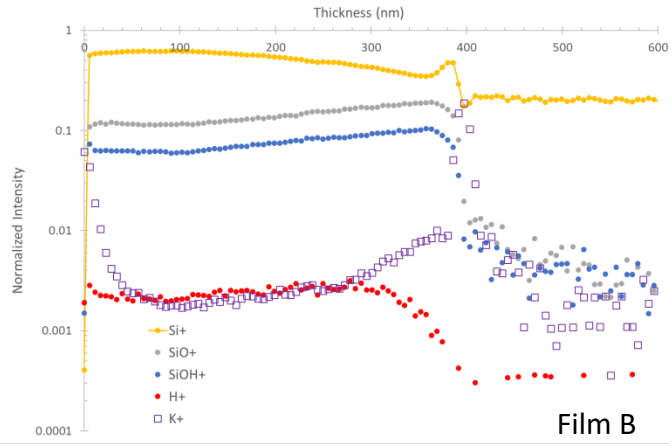

Table 3:????? Mean intensities ratio calculated for the films at t_3

	Film A	**Film B**	**Film C**

$SiOH^+/SiO^+$	0.61	O.55	0.49
$H^+/SiOH^+$	0.030	0.034	0.030
K^+/H^+	2.7	0.9	0.3

Film C

Figure 4: TOF-SIMS depth profiles of samples A (a), B (b) and C (c), all recorded at t_3.

FTIR spectra (figure 5) were recorded before and after the alteration experiment (t_0 and t_3). All spectra are commented for two main areas. A first area is situated between 800 and 1300 cm^{-1} and dominated by the vibrational modes corresponding to the Si-O-Si chemical bond [33]: the asymmetric stretching mode TO3 appearing at 1080 cm^{-1} and its corresponding longitudinal optical vibration mode LO3 at around 1240 cm^{-1} (when recorded at 60°)[34]. TO3 is more intense for sample C since it is the thickest one but also it is supposed to have a denser initial network due to the higher temperature of deposition. The transverse optical bending mode TO2 appears at 800-820 cm^{-1} [35] and the vibration of Si-OH band is seen at 935 cm^{-1} [36]. A second zone situated in the range 2800 to 3700 cm^{-1} holding hydration species absorption bands, namely silanol appearing at 3650 cm^{-1} and the broad band of adsorbed molecular water H_2O with a maximum standing out at around 3400 cm^{-1} [37]. FTIR spectra show that for a same film, the network evolves throughout the alteration experiment. This evolution is proven by the variation of band positions and intensities from pristine to altered sample [38-39]. Indeed, it is clearly observed in figure 5-a that, for A, the intensities of TO3 and TO2 bands decrease remarkably after alteration, Si-OH and water vibrations follow the same tendency. For film C, as shown in figure 5-c, a decrease in TO2 and TO3 bands intensities is also observed but in a lesser degree than for A. The spectrum of altered C is also interestingly marked by the appearance of Si-OH vibration at 935cm^{-1} and the LO3 signal that starts to appear after being present just as a shoulder at t_0. Molecular water band intensity also increased during alteration. Graph 5-d compares the spectra from the three altered samples (at t_3). Figure 5-e shows for t_3 the TO2 and Si-OH bands intensities and total peak ratio of water (3400 cm^{-1}) to Si–O–Si (TO3) peak versus Td. Film C has the highest TO2 band intensity followed by B and A, however Si-OH intensity follows a reverse order, where the strongest one is observed in A. Bands intensities ratio of water to Si-O-Si (TO3) tends to reduce at higher deposition temperature.

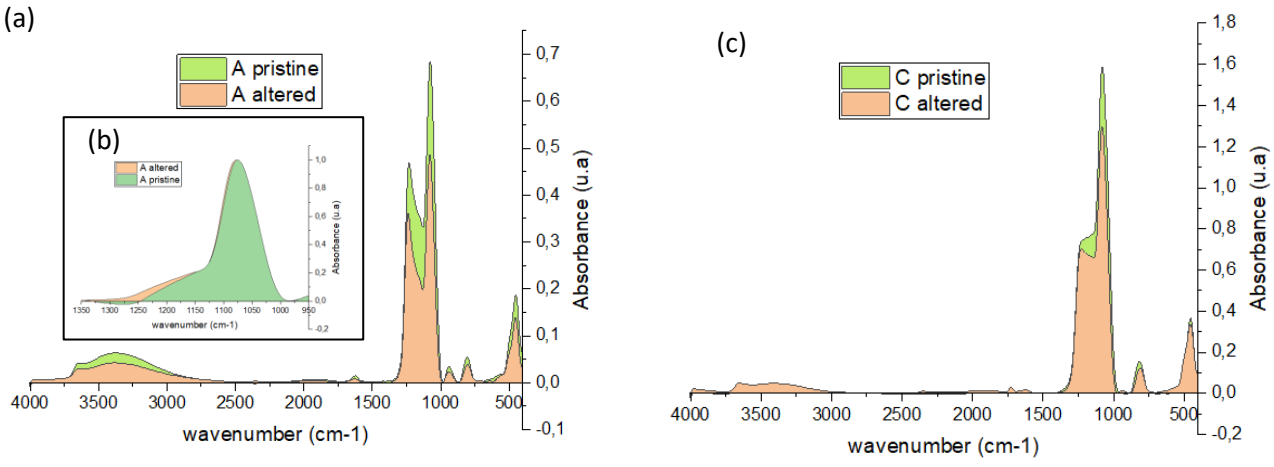

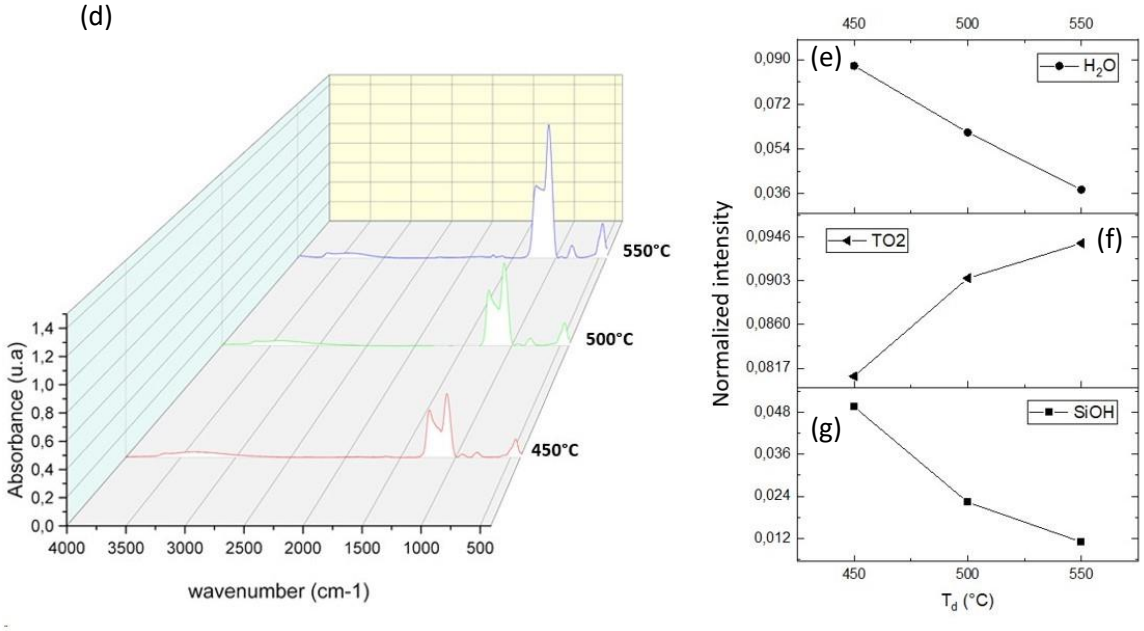

Figure 5: FTIR spectra of films A recorded at a 60° angle (a) and 0° (b) at t_0 (green) and t_3 (orange) alteration. (c) FTIR spectra of film C recorded at a 60° angle at t_0 and t_3. (d) comparison of the FTIR spectra for samples A (red), B (green) and C (blue) at t3, (e) intensity evolution for Si-OH, TO2 and the ratio of water band to Si–O–Si TO_3 band vs deposition temperature of the altered films (t_3).

^{1}H NMR spectrum from sample A altered during t_3, exhibited in figure 9, shows a set of overlapped peaks appearing in the range of chemical shifts going from 0 to 7 ppm. This signal can be divided into two parts corresponding to two different environments of the proton. A first part holding the most intense peaks appearing between 0 and 3 ppm assigned to isolated silanols. A second part with only two broad peaks arising between 3 to 7 ppm that could be attributed to silanol bounded to water molecules or to water molecules strongly bounded to the silicate network. The signal assigned to water molecules at 5 ppm that often dominates the spectrum in altered glasses, appears here very weak [40].

2- Surface state and mechanical properties

AFM surface maps fulfilled at t_3 are illustrated in figure 6. They show, for film C (figure 6c), quite homogeneous smooth surface corresponding to a root mean square roughness (rms) of 0.6 ± 0.1nm, while A (figure 6a) presents a rougher surface with many porosities reflecting a higher rms value of 2.0±0.1nm. An intermediate surface state is observed for B (figure 6b) with a roughness value of 1.7 ± 0.3nm. Further analysis of film A, conducted via SEM, provided a more in-depth examination of its surface characteristics. The backscattered electron (BSE) image displayed in Figure 6d reveals the presence of small, bright spots of nanometric size clustered across the entire surface of the film.

Mapping of silicon (Si) and oxygen (O) distribution (figures 6e-f) accentuates the correlation between these bright spots and an enrichment of oxygen.

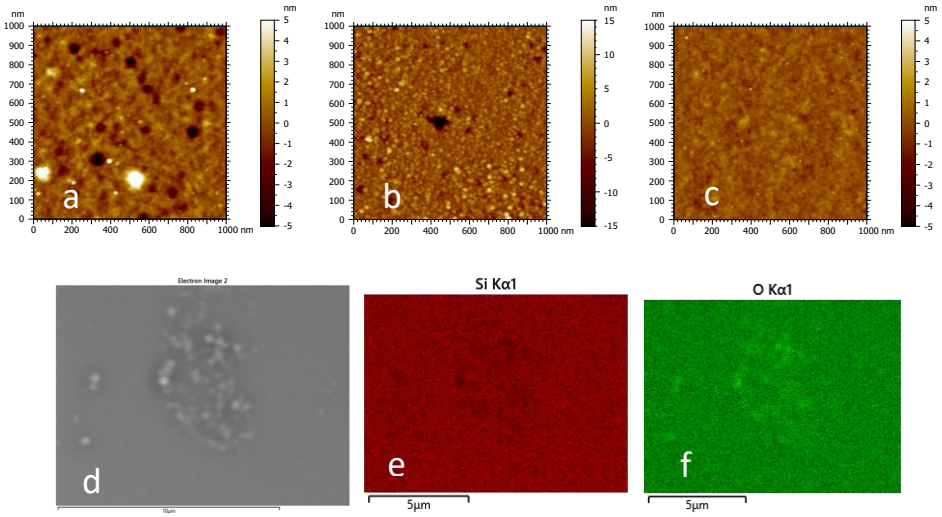

Figure 6: AFM images of films A (a), B (b) and C (c) at t_3, SEM-BSE image of film A at t_3(d) and joint EDX mapping of silicon (e) and oxygen (f)

After complete alteration experiment, nano-indentation tests have led to similar results of Young modulus and hardness for all the films represented respectively by the average calculated values 55.7± 0.9 GPa and 4.5 ± 0.1GPa. Same noting was observed with the pristine films where higher values of mechanical parameters were found as it is shown on figure 7. Thus, altered films recorded a strong drop on the average hardness of about 38%, while the elasticity has decreased by 13% after alteration.

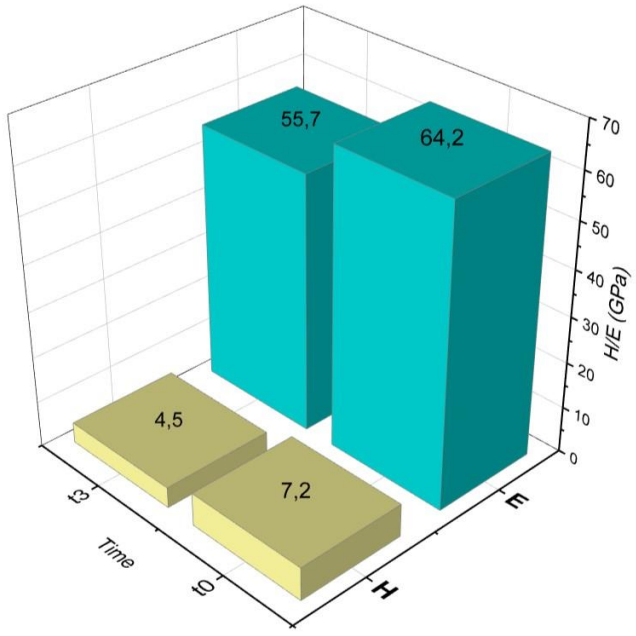

Figure 7: Average values of Young's Modulus (E)and Hardness (H)of the three films before (t_0) and after (t_3) alteration.

Discussion section

Based on prior research [13, 15], silica films deposited via Chemical Vapor Deposition (CVD) using the TEOS/O_2/O_3 route within the temperature range of 400 to 550°C, are anticipated to exhibit characteristics of amorphy, homogeneity, and a low surface roughness typically ranging from 0.4 to 0.5 nm. These films are known to possess excellent structural integrity. Consistent with these findings, detailed assessments conducted via Ion Beam Analysis (IBA) and Infrared Thermal Imaging (IRTF) on the pristine coatings synthesized at Td of 450°C, 500°C, and 550°C initially demonstrated a further improvement in film quality with increasing Td. Notably, the measured O/Si ratios range between 1.98±0.01 at 450°C and 2.18±0.01 at 550°C, compared to 1.93±0.01 at 400°C and 2.24±0.01 at 550°C as reported in a previous study [15]. Additionally, the hydrogen content is determined to be 7.2±0.2% in film A (450°C), 5.8±0.2% in B (500°C), and 4.3±0.1% in C (550°C), compared to 7.8 at.% and 4.5 at.% respectively at 400°C and 550°C according to the same study [15]. These measured O/Si and H levels align entirely with the anticipated values. Furthermore, IRTF spectra reveal significant splitting in TO3 / LO3 and intensified TO2 vibration, the intensity of which escalates with deposition temperature, indicating a heightened degree of silica network polymerization influenced by deposition temperature. Despite the detected chemical and structural differences between films A, B, C, it is important to emphasize that all of them have a high quality network. Thus, comparing their behavior during chemical alteration is crucial to establish links between these slight structural and compositional differences and their chemical and mechanical performances.

During successive alterations of approximately 9 months in KOH aqueous solution with pH adjusted to 4, the samples have been characterized using numerous tools to obtain information on the macroscopic and microscopic changes that could occur. Surface characterization by AFM has highlighted an increased RMS roughness at t_3 compared to t0 for the three films. The alteration has more affected the surface of film A and especially, created pores that are quite visible on the images with a mean width of approximately 50 nm and a depth of some nanometers. The retained RMS of 2.0 nm reflects the balance of these irregularities (peaks/pores). This is a proof that film A was affected by the solution through silica dissolution. In a lesser degree, B film's surface was affected, having thus a moderately large porosity with a width around 10 to 20 nm and a lower RMS value of 1.7 nm. However, sample C surface remains very smooth and homogeneous with extremely small nanoscopic pores that cannot be resolved by AFM, RMS value retained is 0.6 nm, which underscores its higher chemical resistance [41]. Further exploration of sample A surface at t_3 by SEM-EDX reveals the presence of white spots distributed all over the surface and corresponding to an oxygen enriched composition compared to the surrounding area corresponding to silica (figure 6). These observations can be explained by the adsorption of molecular water (hydration) and the generation of depolymerized areas through formation of silanol bonds (hydrolysis).

According to IBA characterizations, all the films have experienced a noticeable thickness loss. However, film A has the most important loss of 157 ± 1.4 nm compared to B and C that lost respectively 151± 1.4 nm and 141± 1.4 nm at t_3. These thickness losses are the result of dissolution of silica in the solution [42]. Hydrolysis of Si-O-Si linkages is the main step controlling the dissolution of silica network [43]. In

fact, water molecules near the film surface start reacting with adjacent Si-O-Si bridges by breaking them, leading to the formation of Si-OH groups:

$$\equiv Si - O - Si \equiv \ + H_2O \rightleftharpoons \ 2 \ \equiv Si - OH \qquad (3)$$

This reaction is repeated until the splitting of all the Si-O-Si bonds of a same silicon atom resulting in the release of H_4SiO_4 in the solution. However, the probability of occurrence of this hydrolysis reaction is strongly depending on its corresponding energy barrier, which is directly linked to the connectivity of the silicon atom to the solid. As a matter of fact, A. Pelmenschikov estimated dissociation energies for the double-, triple- and quadruple-linked Si species to be 23, 33 and 49 kcal/mol respectively [44]. Thus, the larger the number of Si-O-Si bonds for a same silicon atom, the stronger the resistance of the film to hydrolysis. This assumption can explain the variation of thickness losses of our films given the enhancement of the network polymerisation by the deposition temperature. Therefore, films produced at higher temperatures are denser and mainly constituted of Q^4 tetrahedra (filmC), hence, will resist more to the dissolution [45]. This same assumption can also elucidate the discrepancy in the initial thickness loss rate values among the three films, as depicted in Figure 2-b, ranging from 2.5 nm/day for C to 4.8 nm/day for A. This discrepancy can be attributed to the robust resistance of films deposited at higher temperatures, which retards the dissociation mechanism [46]. It is worthy to note that the removal of H_4SiO_4 units seems to be happening evenly all over the surface as evidenced by the consistent thickness measurements obtained from various probed positions on the altered films, particularly for film C. This uniformity in thickness suggests that all sites within the upper surface of the coatings exhibit a similar reactivity, contributing to the even removal of H_4SiO_4 units. AFM images can confirm this observation as roughness is still quite low. It is worth mentioning that despite the observed reduction in thickness, the initial rates of thickness loss in our films are relatively low compared to the sparse reported values of silica films thickness loss rates in the literature, which typically range from 0.1 to 50 nm/h [20].

The chemical composition of the films measured at t_0, t_1, t_2 and t_3 using IBA analyses (Table 2) highlights the dependence of hydrated species progression on Td. The measured hydrogen concentration increases during the first days of alteration for all the films but is still rather quite low, the highest level was measured in film A at t_1 where it reached 9.10 ± 0.29%. After t_1, as it was mentioned in results section, dissimilar behaviours were noticed, particularly for film A that has shown a decrease in hydrogen content to reach 7.13 ± 0.24 at.% at t_3. It must be noted that the concentration measured in film C at t_3 is lower than the initial concentration (t_0) in sample A. It is probable that a cyclic process leads to the gradual hydration then dissolution of a highly hydrated extreme surface, resetting the diffusion process. As illustrated by the ERDA profiles of sample C, the initial polymerisation degree of silica is a key parameter to establish an efficient barrier to the water diffusion and to hydrolysis. Considering the O/Si ratio, surprisingly the values at t_3 are rather stable during alteration and comparable to pure silica, namely2.10 : 1.96 : 2.12 respectively for samples A:B:C.

IRTF spectroscopy was used to highlight network evolution throughout alteration and this analysis is particularly rich to describe the network of such systems. Before discussing IRTF results, we have to comment on the shape of LO3 band of pristine film C that appears as a shoulder rather than a complete band despite the fact that we were working at 60° off normal. According to the literature, the thickness of the sample affects the TO3 and LO3 bands intensities. In fact, J.A. Moreno et al working with an incident angle of 45° have shown that the intensity of TO3 band evolves linearly with film thickness, whereas the LO3 band intensity follows an exponential evolution, which means that for thicknesses

beyond 500 nm as shown on figure 8-b, the gap between the two intensities becomes significant and affects the shape of the spectrum in the concerned area [46]. To adapt this observation to our own samples, 3 additional films have been dedicated to this study. They have been deposited in exactly the same conditions (Td = 550°C) except the deposition time, which leads to similar silica networks with different thicknesses ranging between 80 and 750 nm. As shown in figure 8-a, the intensities ratio of LO3 to TO3 decreases significantly with the film thickness. Our values appear to be very close to those obtained by Moreno, and we verified that the small gap in bands intensities is due to the difference of the used incident angles (45° for Moreno against 60° for us). LO3/TO3 ratio also depends on the incident angle as shown in figure 8-c.

Regarding the film A alteration results, the decrease in TO3 intensity recorded between t_0 and t_3 can be interpreted by network depolymerisation via hydrolysis and conversion of siloxane into silanol, but mainly by network dissolution since the signal intensity is very sensitive to the oscillator number and so to the coating thickness. The decrease of TO2 band intensity for the same film would translate to a decrease in the number of chemical bonds between SiO_4 tetraedra and so to network depolymerisation [47]. Similar observations were made for film C, where a less pronounced decrease in TO3 and TO2 band intensities was observed. Additionally, a new band at 950 cm^{-1} corresponding to Si-OH appeared, a feature not present in the spectrum of the pristine film, which indicates a small depolymerisation giving birth to Q^3 or probably both Q^3 and Q^2 tetrahedra [40;48]. Contrary to A, sample C has recorded an increase in the adsorbed water reflected by a stronger band around 3400 cm^{-1}. LO3 band at around 1230 cm^{-1} becomes more visible after alteration, which is thought to be due to thickness decrease effect as mentioned above.

For film A, the unexpected reduction of the Si-OH and water bands intensities after alteration can be explained by two facts: first of all, the stronger and faster network dissolution compared to the other samples that automatically reduces the water and silanol content in the sample by leaching H_4SiO_4. Secondly, the ToF-SIMS results have shown the presence of potassium in the three samples, occurring by cation diffusion coming from the solution via ion exchange with protons of the network (equation (4)) [49]. TOF-SIMS depth profiling (figure 4) upholds this finding by exhibiting the penetration of potassium to a larger extent in film A. Minor quantities of potassium were also detected in B and C reflecting a fractional cation exchange, which is directly related to the initial incorporation of hydrogen through hydrolysis (K^+/H^+= 2.7 for A against only 0.3 for C). In fact, since film A is the most attacked, it is supposed to develop large enough pores (confirmed by AFM) that permit a more massive penetration of such voluminous K^+ cation via ion exchange with protons. In agreement with Almeida et al., this rise of porosity is confirmed on the 0° IRTF spectrum by the rising of the shoulder appearing at 1200 cm^{-1} (figure 5-b) after alteration (t_3) [50] .

$$Si - OH_{(s)} + K^+_{(aq)} \rightleftharpoons Si - OK_{(s)} + H^+_{(aq)} \quad (4)$$

Furthermore, the decrease in Si-OH bonds due to ion exchange will provoke a decrease in the amount of adsorbed water bonded to Si-OH via hydrogen bonding, which explains the drop of the adsorbed molecular water band intensity too. This phenomenon of ionic exchange will occur in a lesser degree for B and C since they are fewer affected by the aqueous corrosion and that is probably why it was not detected by IRTF. Despite this, as shown in figure 5-e, film A at $t_3$still exhibits the strongest Si-OH band and the weakest TO2 compared to the other samples. It also possesses the topmost intensity band ratio of water to TO3 while C has the smallest one. This shows the different levels of alteration of our

coatings. Thus, the intensity of the high frequency band relative to hydration species is dependent on a competition between hydrolysis (equation 3) and ionic exchange (equation 4).

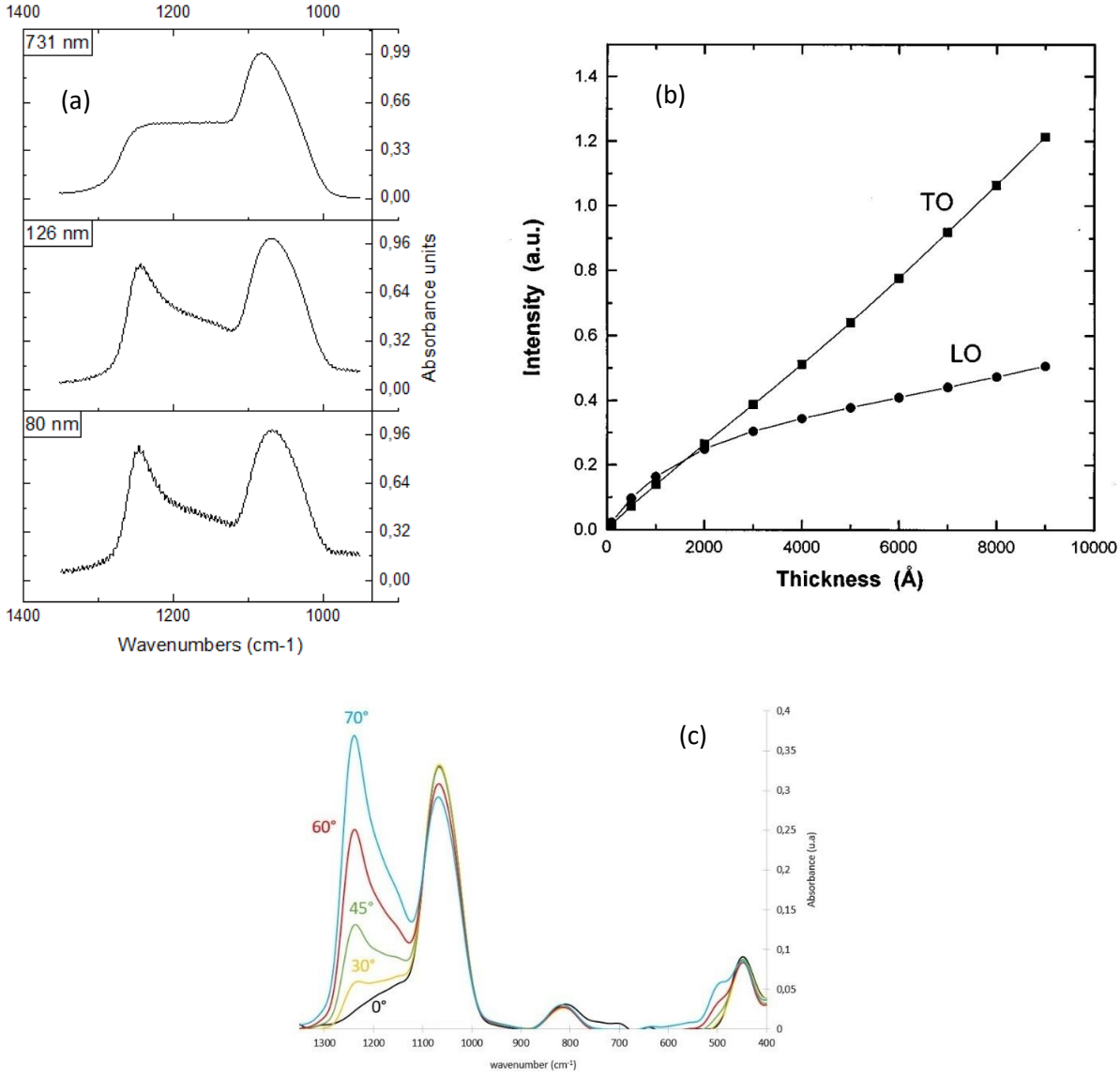

Figure 8: (a) TO3 and LO3 bands intensities recorded at 60° for silica coatings with different thicknesses, (b) evolution of LO3-TO3 intensities at 45° off normal with thickness given by Moreno et al.[46]and (c) evolution of the FTIR fingerprint spectrum with incident angle.

^{1}H NMR spectrum for sample A (at t_3) confirms the very low hydrogen content in the film, as measured by ERDA, ToF-SIMS and IRTF. Signals deconvolution showed that the strongest peaks appearing between 0.12 and 1.31 ppm correspond to isolated silanol that could be located in the depth of the layer. On the other hand, there are two broad weak peaks that could be assigned to silanol bounded to water molecules or to water molecules strongly bounded to the silicate network that should be located at the extreme surface of the film. This is in agreement with ERDA depth profiles that show a lower hydrogen level at the film surface and tends to rise inside the sample.

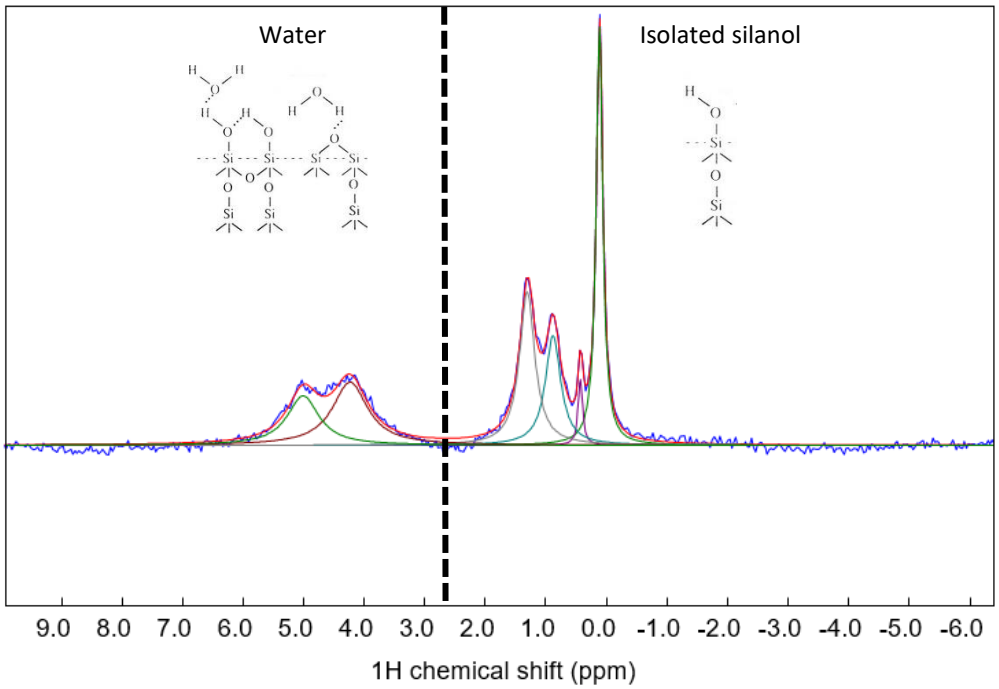

Figure 9: ^{1}H MAS NMR signal obtained on altered film A at t_3 at 750 MHz.

Table 3: peaks positions, widths and intensity of the ^{1}H MAS NMR signal of film A at t_3, recorded at 750 MHz.

Chemical shift (ppm)	0.12 ± 0.1	0.43 ± 0.1	0.88 ± 0.1	1.31 ± 0.1	4.23 ± 0.1	5.01 ± 0.1
Width (ppm)	0.13	0.09	0.31	0.31	0.71	0.64
Intensity (%)	26	3	15	22	20	14

The average measured values of the mechanical properties for the three films have decreased during the alteration process. However, despite their chemical and structural differences, the altered films exhibit similar hardness and elastic modulus values. The drop of about 13% in Young's modulus suggests that the films did not develop significant defects such as pores, fractures, or cracks [51-52]. This result aligns with the low content of hydration species and the limited network depolymerisation

observed during the alteration experiments, but also the relatively low rms values measured at t_3. In the case of film A, the presence of K^+ ions likely contributes to reinforcing the coating through chemical quenching, compensating for the lower quality of the silica network compared to film C. However, the significant 38% decline in hardness indicates that the extreme surface has been strongly modified. Consequently, the strength of the intermolecular bonds within the network is weakened, likely due to the creation of new non-bridging oxygen, which affects their resistance to deformation. Hardness is known to be highly sensitive to the extent of cross linking in the material, explaining the observed decline in this mechanical property [53-54].

Conclusion

In this study, we monitored the gradual evolution of three amorphous silica films, each characterized by a distinct initial network quality, considering structural and chemical properties. Through the combined use of ERDA depth profiles established during the alteration process and IR analyses, we were able to precisely observe the hydration and hydrolysis dynamics within our films. Moreover, we quantified the dissolved thicknesses from each film and derived dissolution rates by analysing and simulating RBS spectra. Initially, dissolution rates were found to range between 2.8 and 4.5 nm/day, stabilizing around 0.4-0.5 nm/day. These findings represent the first available dataset on dissolution rates of silica films deposited via atmospheric pressure CVD. A diffusion of potassium via an ionic exchange with protons has been identified and its intensity is remarkably correlated with the initial network quality. Furthermore, we delved into other pertinent aspects of the study. For example, we underscored the extent of structural modifications on mechanical properties, particularly highlighting the significant impact on hardness due to its close association with network connectivity. In contrast, Young's modulus exhibited a slight decrease, indicative of the network relative stability and creation of few defects, in agreement with the O/Si ratio still being close to 2. This hypothesis is substantiated by surface characterizations, which revealed a remarkably smooth surface even after 279 days of alteration, with the maximum roughness measured at 2nm.

Acknowledgements

The present work was partly funded by ANR (Agence Nationale de la Recherche) under the contract HEALTHYGLASS ANR-17-CE08-0056.

References

[1] S. Dzioba and R.Rousina. Dielectric thin film deposition by electron cyclotron resonance plasma chemical vapor deposition for optoelectronics. Journal of Vacuum Science & Technology B: Microelectronics and Nanometer Structures 1994, 12 (1) 433-440.

[2] T. L. Chu. Dielectric Materials in Semiconductor Devices. Journal of Vacuum Science & Technology1969, (6) 25-33.

[3] N. Carmona, M.A. Villegas, J.M. Fernández Navarro. Protective silica thin coatings for historical glasses. Thin Solid Films 2004, (458)121–128

[4] M. Puyo, K.C. Topka, B. Diallo, R.Laloo, C.Genevois, P. Florian, V.Turq.Beyond surface nanoindentation: Combining static and dynamic nanoindentation to assess intrinsic mechanical properties of chemical vapor deposition amorphous silicon oxide (SiOx) and silicon oxycarbide (SiOxCy) thin films. Thin Solid Films2021, 735, 138844.

[5]S. Ponton, F. Dhainaut,H. Vergnes, D. Samelor, D. Sadowski, V.Rouessac, H. Lecoq, T. Sauvage, B. Caussat, C. Vahlas. Investigation of the densification mechanisms and corrosion resistance of amorphous silica films. Journal of Non-Crystalline Solids, 515, 2019, 34–41.

[6]N.B. Dahotre, P.Kadolkar and S.Shah. Refractory ceramic coatings: processes, systems and wettability/adhesion 2001, 31(7), 659–672.

[7]J.E. Crowell. Chemical methods of thin film deposition: Chemical vapor deposition, atomic layer deposition, and related technologies. Journal of Vacuum Science & Technology A: Vacuum, Surfaces, and Films, 2003, 21(5), S88–S95.

[8]M. M. IslamRaja, C. Chang, J. P. McVittie, M. A. Cappelli, and K. C. Saraswat. Two-precursor model for low-pressure chemical vapor deposition of silicon dioxide from tetraethylorthosilicate. Journal of Vacuum Science & Technology B: Microelectronics and Nanometer Structures 1993, 11(3), 720–726.

[9]M. E. Coltrin; P. Ho, H. K. Moffat and R.J. Buss. Chemical kinetics in chemical vapor deposition: growth of silicon dioxide from tetraethoxysilane (TEOS) 2000, 365(2), 251–263.

[10]K.Okuyama,T. Fujimoto, T. Hayashi and M. Adachi. Gas-phase nucleation in the tetraethylorthosilicate (TEOS)/O3 APCVD process, 1997, 43(Supplement 11A), 2688–2697.

[11] L. Skuja, K. Kajihara, M. Hirano, H. Hosono. Oxygen-excessrelated point defects in glassy/amorphous SiO2 and related materials. NuclInstrum Methods Phys Res B 2012; 286:159-68.

[12] S. Horita andP. Jain. Dependences of deposition rate and OH content on concentration of added trichloroethylene in low-temperature silicon oxide films deposited using silicone oil and ozone gas. Jpn J Appl Phys 2018, 57(3S1). 03DA02-7.

[13] K.C. Topka, G.A. Chliavoras, F. Senocq, H. Vergnes, D. Samelor, D. Sadowski, C. Vahlas, B. Caussat. Large temperature range model for the atmospheric pressure chemical vapor deposition of silicon dioxide films on thermosensitive substrates. Chemical Engineering Research and Design 2020, 161, 146–158.

[14] T. Nishiguchi, S. Saito, N. Kameda, M. Kekura, H. Nonaka andS. Ichimura. Improvement in chemical-vapor-deposited-SiO2 film properties by annealing with UV-light-excited ozone. Jpn J Appl Phys 2009,(48)116509, 1-5.

[15]B. Diallo, K. C. Topka, M.Puyo, C. Lebesgue, C.Genevois, R.Laloo, D.Samelor, H. Lecoq, M.Allix, H. Vergnes, F.Senocq, P. Florian, V.Sarou-Kanian, T.Sauvage, M.J. Menu, B. Caussat, V.Turq, C.Vahlas, N. Pellerin. Network hydration, ordering and composition interplay of chemical vapor deposited amorphous silica films from tetraethyl orthosilicate. Journal of Materials Research and Technology 2021, (13) 534-547.

[16] S. Gin, J.M. Delaye, F.Angeli, S. Schuller.Aqueous alteration of silicate glass: state of knowledge and perspectives. npj Materials Degradation2021 (42).

[17] F.K. Crundwell.On the Mechanism of the Dissolution of Quartz and Silica in Aqueous Solutions. ACS Omega 2017, 2(3), 1116–1127.

[18]Gin, S.; Delaye, J.-M.; Angeli, F.; Schuller, S. Aqueous alteration of silicate glass: state of knowledge and perspectives. npjMater.Degrad. 2021, 5, No. 42.

[19] Pliskin WA. Comparison of properties of dielectric films deposited by various methods. J Vac Sci Technol1977;14:1064e81.

[20]M. Klause; U. Rothhaar; M. Bicker; W. Ohling(2010). Dissolution of thin SiO2-coatings – Characterization and evaluation. , 356(3), 0–146.

[21] C. Moore, T.S. Perova, B. Kennedy. Study of Structure and Quality of Different Silicon Oxides Using FTIR and Raman Microscopy, Proceedings of SPIE, Opto-Ireland 2002, Optics and Photonics Technologies and Applications.

[22]I.I. Shaganov, T.S. Perova, R.A. Moore and K. Berwick, Spectroscopic characterisation of SiO and SiO2 solid films: Assignment and local field influence, J.Material Science: Materials in Electronics, 2001, 12; 351-355.

[23]J.E. Olsen and F. Shimura. Infrared spectroscopy of thin silicon dioxide on silicon, Appl.Phys.Lett., 1988. 53; 1934- 1936.

[24]I.W. Boyd and J.I.B. Wilson. A study of thin silicon dioxide films using infrared absorption techniques, J.Appl.Phys., 1982. 53, 4166-4172.

[25]G. Lukovsky, M.J. Mantini, J.K. Srivastava and E.A. Irene. Low-temperature growth of silicon dioxide films: a study of chemical bonding by ellipsometry and infrared spectroscopy, J.Vac.Sci.Technol, 1987, B5, 530-537.

[26]H. Scholze. Glass-water interactions. Journal of Non-Crystalline Solids, 1988, 102, 1-10.

[27]M.Mayer.SIMNRA, a simulation program for the analysis of NRA, RBS and ERDA, AIP Conf. Proc. 1999 ; 475, 541.

[28]Martin et al., Nuclear Instruments and Methods in Physics Research B 258 (2007) 471–478

[29]P. Lange, W. Windbracke, Characterization of Thermal and Deposited Thin Oxide Layers by Longitudinal Optical-Transverse Optical-Excitation in Fourier-Transform IR Transmission Measurements, Thin Solid Films,1989, 174 : 159-164.

[30] B. Harbecke, B. Heinz, P. Grosse, Optical-Properties of Thin-Films and the Berreman Effect, Appl Phys A: Mater Sci Process, 1985,38: 263-267.

[31] Massiot D. dmfit program; available at http://crmht-europe.cnrsorleans.fr

[32]R. Saha; W.D. Nix. Effects of the substrate on the determination of thin film mechanical properties by nanoindentation. Acta Materialia 50 (2002) 23–38.

[33]S.N. Taraskin, S.R. Elliott, Nature of vibrational excitations in vitreous silica, Phys Rev B, 56 (1997) 8605-8622.

[34]B. Harbecke, B. Heinz, P.Grosse. Optical properties of thin films and the Berreman effect, Appl Phys A , 38 (1985) 263-267.

[35] P. Innocenzi.Infrared spectroscopy of sol–gel derived silica-based films: a spectra-microstructure overview, Journal of Non-Crystalline Solids 316 (2003) 309–319.

[36] A. Milella, F. Palumbo, J.L. Delattre, F. Fracassi, R. d'Agostino, Deposition and characterization of dielectric thin films from allyltrimethylsilane glow discharges, Plasma Processes and Polymers, 4, 2007, 425-432.

[37]Alfred A. Christy, Per K. Egeberg. Quantitative determination of surface silanol groups in silicagel by deuterium exchange combined with infrared spectroscopy and chemometrics. The Analyst, 130(2005), 738–744.

[38]A. Oufakir, L. Khouchaf , M.Elaatmani , A. Zegzouti , G. Louarn and A. Ben Fraj, Study of structural short order and surface changes of SiO2 compounds, MATEC Web of Conferences 149, 01041 (2018).

[39]P. Innocenzi and P. Falcaro, Order-Disorder Transitions and Evolution of Silica Structure in Self-Assembled Mesostructured Silica Films Studied through FTIR Spectroscopy, J. Phys. Chem. B (2003), 107, 4711-4717.

[40]M.Collin, B.Diallo, H.Lecoq,S.Ory, E.Chauvet, N.Pellerin, (2020). Chemical durability of lead crystal glass: comparison of short-term aqueous and atmospheric alteration at 90 °C. Int J Appl Glass Sci. 2020;00:1–17.

[41] A.B. Jedlicka and A.G. Clare, Chemical durability of commercial silicate glasses. I material characterization, Journal of Non-Crystalline Solids 281 (2001) 6-21.

[42]H. Scholze, Glass-water interactions, Journal of Non-Crystalline Solids 102 (1988) 1-10.

[43]T.R. Walsh, M. Wilson and A.P. Sutton, Hydrolysis of the amorphous silica surface. II. Calculation of activation barriers and mechanisms, J. Chem. Phys, 2000, (113) 9191-9201.

[44]A. Pelmenschikov, J. Leszczynski and L. G. M. Pettersson. Mechanism of Dissolution of Neutral Silica Surfaces: Including Effect of Self-Healing, J. Phys. Chem. A (2001), 105, 9528-9532.

[45] P.M. Dove, N. Han, A.F. Wallace and J. De Yoreo.Kinetics of amorphous silica dissolution and the paradox of the silica polymorphs, Proceedings of the National Academy of Sciences, 105(29), 2008, 9903–9908.

[46] J.A. Moreno et al, J. Appl. Phys. 81 (1997)

[47]S. Gin, J.M. Delaye, F. Angeli and S. Schuller. Aqueous alteration of silicate glass: state of knowledge and perspectives, npj Materials Degradation (2021) 42.

[48]D. De Sousa Meneses, M. Eckes, L. del Campo, C.N. Santos, Y. Vaills, P. Echegut, Investigation of medium range order in silicate glasses by infrared spectroscopy, VibSpectrosc, 65 (2013) 50- 57.

[49] L. H. Allen and E. Matigevic, Stability of colloidal silica, Journal of Colloid and Interface Science, 33(3), 1970.

[50] R.M. Almeida and C.G. Pantano, Structural investigation of silica gel films by infrared spectroscopy. J. Appl. Phys, 1990, (68) 4225-4232.

[51]S. Wei, F. Qun-Bo, W. Fu-Chi and M. Zhuang, The influence of defects on the effective Young's modulus of a defective solid, Chin. Phys. B, 22(4),2013, 044601 1-5.

[52] A. G. Kvashnin, P. B. Sorokin anf D. G. Kvashnin, The Theoretical Study of Mechanical Properties of Graphene Membranes, Fullerenes, Nanotubes and Carbon Nanostructures, 2010, 18:4-6, 497-500

[53] John J. Gilman, Chemistry and Physics of Mechanical Hardness 2009.

[54]M. Yamane and J.D. Mackenzie, Vicker's hardness of glass, Journal of Non-Crystalline Solids, 15 (1974) 153-164.